

Ring-shaped array ultrasound imaging using ellipse algorithm

Liu Yang, Chunguang Xu*, Xianghui Guo

Key laboratory of Fundamental Science for Advanced Machining, Beijing Institute of Technology, Beijing, China, 100081

Received 6 October 2014, www.cmnt.lv

Abstract

A ring-shaped array tomography modal consists of 36 ultrasonic transducers is established to study the multi-objects imaging in fluid medium by the ellipse algorithm. The algorithm is based on ultrasonic reflection mode which is a good alternative to transmission tomography when the inspected object would bring about severe attenuation to ultrasound. Ultrasonic propagation inside the ring-shaped array is simulated by COMSOL Multiphysics® software. Air bubbles and solid objects are insonified separately by the propagating waves and the corresponding scattering waves are detected through the ring-shaped array transducers. After the superposition of the numerous ellipses and threshold filtering for the reconstructed images, the shapes, sizes and positions of the tested objects are successfully reproduced.

Keywords: Ultrasonic Tomography; Ring-shaped Array; Ellipse Algorithm

1 Introduction

Ultrasonic Computed Tomography (UCT) gives the opportunity of quantitative and real-time imaging in chemical industrial process [1]. It has advantage of imaging two phase component flow such as oil/water or gas/water mixture since UCT enables the inspection of certain characteristics of objects that cannot be easily obtained by other methods [2]. The cross-section images of the two phase flow provide the identification information of the mixing zone distribution and the interface of the component in order to improve the process control [3].

Besides industrial applications, UCT is also extensively used in the area of clinical medicine. Compared with X-ray tomography [4-6], the clinical tissue mapping quality of UCT is still unable to rival its counterpart [7] in terms of the ability to distinguish tissue pathologies. But UCT can be preferred to the classical X-ray mammography if the theoretically possible resolution of UCT in tenths of a mm is reached [8]. The resolution of UCT is mainly limited by the artifacts due to diffraction effects in strong inhomogenous media, the quantitative reconstruction is only possible for a non-applicable restrictive domain [9] because that Born and Ritov approximations are not valid in general condition. For improving the reconstruction quality, Many types of reconstruction methods such as diffraction tomography[10], transmission tomography [11-13] and reflection tomography [14-16] have been applied to the medical imaging. An UCT system for early breast cancer diagnosis is developed at Karlsruhe Institute of Technology [17-20], in the research and development process, A field-programmable gate array (FPGA)-based data acquisition system is used to acquire the raw data of 20GB each time [17]. An Eikonal solver that can calculate the bent ray paths for the transmission pulses is applied to improve the algebraic reconstruction technique which relies on the assumption that the transmission rays propagate straight from emitter to receiver [11].

In this paper reflection mode UCT is selected to reconstruct the multi-objects images under the assumption

of little change of refractive index. When the region of interest is naturally shadowed by certain material that would bring about severe attenuation to ultrasonic energy, transmitted pulses almost completely reflect and give null signals to the receive transducer that located on the opposite direction [16]. On this occasion, reflection mode can be a better solution. In order to obtain the reflection signals from every possible angle, an immersion array with 36 transducers is arranged in a ring-shape. In this way, an extensive dataset is provided from which the spatial distribution of the ultrasonic propagation parameters can be reconstructed using a suitable inversion procedure.

Firstly, the simulation and experimental model of ring-shaped array system is established. Secondly, the method of the reflection tomography and the image reconstruction algorithms are described. Thirdly, the propagation of the ultrasonic wave as well as the interaction between the objects and the ultrasonic wave are all numerically simulated by COMSOL Multiphysics® software. After that, images of air bubbles and solid multi-objects are reconstructed through the elliptic curve algorithm. Image qualities are improved by the aid of threshold filtering. At last, the feasibility and reliability of the immersion array system are discussed.

2 Model

2.1 SYSTEM SET-UP

Generally, the imaging process of an UCT system consist of two main steps. The first step of UCT is mainly realized through hardware. Transmitting and receiving are implemented by the array transducers controller. Multi-channel ultrasonic board is employed to generate pulses which have the same frequency to array transducers. The ultrasonic sensors are used as both transmitters and receivers. When receiving the ultrasonic waves, a band pass filter is needed to get rid of a proportion of noise and some received signals that are of low energy have to be amplified for further analysis. In the second step the received data are

* Corresponding author e-mail: xucg@bit.edu.cn

combined to gain the reconstructed image through inversion procedure. Signal processing and pixel value calculating of the reconstructed image are achieved by mathematical software. Figure 1 shows the block diagram of the UCT system.

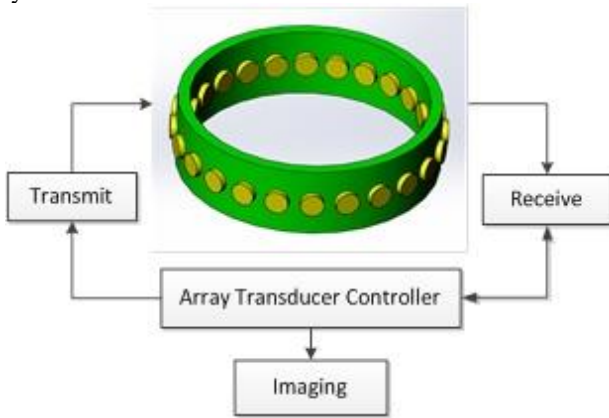


FIGURE 1 The block diagram of the ultrasonic computed tomographic system

The imaged objects are placed in a ring-shaped container (the bottom of the container is omitted. see Figure 1) filled with water as a coupling medium and 36 transducers are embedded in the same axial distance around the circumference of the container whose diameter is 100mm. Each transducer is of 0.5MHz frequency and 5mm width diameter. The received signals are sampled at 10MHz for $100 \mu s$. Objects inside the ring-shaped array are insonified by a fan-shaped radiation fired from a single transducer while the ring-shaped array system allows the signal to be detected and measured individually. The pulse firing and the signals receiving are carried out in sequence, thus the reconstruction data can also be collected in order. The ring-shaped array and the configuration of the propagation are sketched in Figure 2.

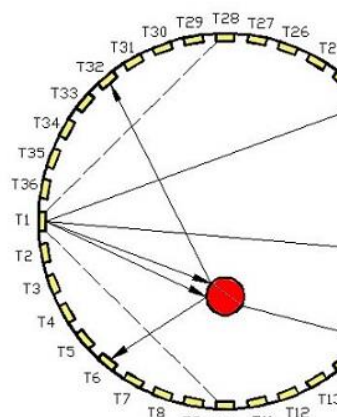


FIGURE 2 The configuration of ultrasonic propagation inside the ring-shaped array. A fan-shaped beam is emitted from one transducer and then scattering occurred when ultrasonic wave is getting through the object. Signals will either directly transmit across the detection region or reflect from the target

2.2 REFLECTION METHOD

In transmission mode, the efficiency of data collection is

limited by the acoustic impedance mismatch, for instance, air-bubbles mixed in the water medium make it difficult for the ultrasonic wave to get to the receiver in the opposite side. To overcome this problem, reflection mode is selected to obtain more effective signals and the multi-position signal receiving method is employed to minimize the data acquisition time.

Amplitudes and phases of the ultrasonic wave are influenced by the interactions between the incident wave and the objects to be imaged when the ultrasonic wave is propagating.

The interactions can be presented by acoustic impedance:

$$Z = \rho c [21], \tag{1}$$

where ρ is the material density, c is the speed of sound and Z is the acoustic impedance of the medium.

Homogeneous medium only causes the amplitudes decline, but the interfaces can alter both the amplitudes and the phases of the incident wave to a remarkable extent. It is clear that the greater the difference in impedance at the interface, the greater the amount of energy that will be reflected.

The reflection coefficient R and refraction coefficient D can be defined as:

$$R = \frac{P_r}{P_i} = \frac{\rho_2 c_2 - \rho_1 c_1}{\rho_2 c_2 + \rho_1 c_1} = \frac{Z_2 - Z_1}{Z_2 + Z_1}, \tag{2}$$

$$D = \frac{P_t}{P_i} = \frac{2\rho_2 c_2}{\rho_2 c_2 + \rho_1 c_1} = \frac{2Z_2}{Z_2 + Z_1}, \tag{3}$$

where P_r means the sound pressure of reflected wave, P_t means the sound pressure of incident wave, P_i means the sound pressure of refracted wave or transmitted wave. $Z_1 = \rho_1 c_1$ is the acoustic impedance of material 1, from which the incident wave penetrate the interface, $Z_2 = \rho_2 c_2$ is the acoustic impedance of material 2, into which the incident wave penetrate the interface. The values of R and D depend on the characteristic impedances of the two materials.

This imaging process is based on a finite time waveform analysis including reflection time, amplitudes and phases calculating. The observation time is equal to the arrival time of the first peak after the time-of-flight, as shown in Figure 3.

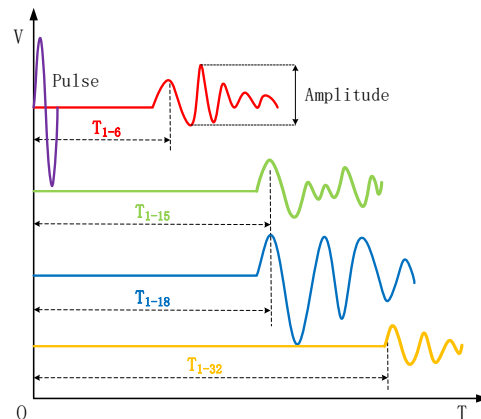


FIGURE 3 Effective receiving signals for different ultrasonic propagation path

In Figure 3, the time-of-flight denoted by T is calculated by means of the distance from the start time of the pulse to the first peak of the received signal. If the objects to be imaged are certain materials with sound hard boundary, such as air bubbles or solid particles, the effective signals can only be received by reflection mode. On the contrary, transmission signals can be received on the opposite side of the pulse transducer. Suppose the object shown in Figure 2 is a bubble, it is much easier to get the reflected signals T_{1-6} and T_{1-32} (see Figure 3). Because of the different ultrasonic propagation paths, the observation time of signal T_{1-6} is earlier than T_{1-32} while the amplitude of signal T_{1-6} is larger than T_{1-32} . Assume that the object is engine oil, the transmitted signal T_{1-15} will be an effective signal, since the transmitted ultrasonic wave refracts and scatters at the interface of the engine oil and water, signal T_{1-15} shows a comparatively complex waveform and the amplitude of it is clearly smaller than signal T_{1-18} due to the energy loss. The direct wave signal T_{1-18} can always be detected as long as there is no obstacle between transmitter and receiver.

2.3 ELLIPSE ALGORITHM

In order to reconstruct the image of the target, ellipse algorithm is employed. Figure 4 shows the geometric parameters of an ellipse. Point A and B are two focuses of the ellipse and C is a point located on the elliptic curve.

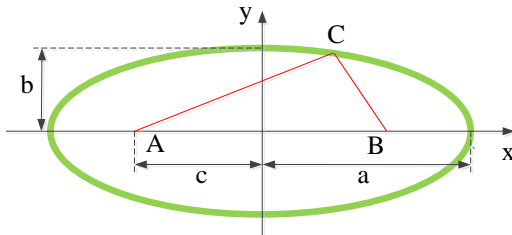


FIGURE 4 Geometric parameters of an ellipse

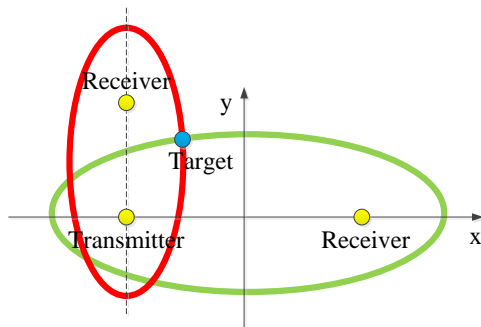


FIGURE 5 Schematic diagram of ellipse algorithm imaging

The following equation derived from the definition of ellipse:

$$AC + CB = 2a . \tag{4}$$

It satisfies any ellipse. In this equation a means the long axis length of the ellipse. Point A and B can be replaced by the transmitting transducer and receiving transducer respectively. Point C can be considered as a certain point on the target which would reflect the ultrasonic pulse. Thus, the sum of AC and CB represents the distance of ultrasonic reflection path from firing to receiving.

As long as the parameter a is obtained, another parameter b can be easily induced from the equation:

$$b = \sqrt{a^2 - c^2} . \tag{5}$$

Here b is the short axis length of the ellipse, c is the focus distance of the ellipse which is exactly the half distance of a pair of transmitting-receiving transducers.

The propagation time of the ultrasonic reflection path can be calculated through the equation:

$$t_{ij}(x_c, y_c) = \frac{1}{c}(AC_i + CB_j) = \frac{1}{c} \left(\sqrt{(x_c - x_i)^2 + (y_c - y_i)^2} + \sqrt{(x_c - x_j)^2 + (y_c - y_j)^2} \right) . \tag{6}$$

The transducer coordinates: x_i, y_i and x_j, y_j have been determined according to our ring-shaped array setup, their subscripts i and j denote transmitting mode and receiving mode of the transducer respectively. When all necessary parameters of an ellipse are obtained, a particular ellipse can be drawn in a determined position and dimension. The target being detected is supposed on the elliptic curve. Theoretically, one single point on the target can be determined by drawing only two ellipses. The schematic diagram of ellipse algorithm imaging is depicted in Figure 5.

In this tomographic system, the effective spatial resolution of the reconstructed image to a great extent depends on the number of transducers. The resolution should be improved with the increase of the transducer number. Since the transducers cannot be rotated, the total number of the signals that can be received is given by:

$$L = N^2 , \tag{7}$$

where L is the total number of the received signals, N is the number of transducers.

According to the reversibility of the ultrasonic path, the effective number of the receiving signals should be reduced to:

$$L = \frac{N \cdot (N - 1)}{2} . \tag{8}$$

If $N(N - 1)/2$ possible sensor pairs are all successfully repeated to get signals, the intensity of location (x_c, y_c) can be given by:

$$I(x_c, y_c) = \sum_{i=1}^{N-1} \sum_{j=i+1}^N d_{ij}(t_{ij}(x_c, y_c)) \tag{9}$$

Here $d_{ij}(t_{ij}(x_c, y_c))$ stands for the amplitudes of the signals scattered from the target point (x_c, y_c) . When this process is repeated for every location on the tested objects then a reconstructed image of the objects is created.

3 Simulation and reconstruction

3.1 SIMULATION RESULTS

COMSOL Multiphysics® software is used to simulate the transient mode ultrasonic propagation. When the ultrasonic

waves traverse the objects, reflection, refraction and diffraction all occurred, so the receiving signals of the transducers are very complex for they are the superposition of multi-interaction between ultrasonic and objects.

The finite element calculation aims to determining the scattering wave of the objects. Figure 6 shows the scattered acoustic pressure distribution of three air bubbles. The

coupling medium inside the ring-shaped array is water and the radii of the air bubbles are 3mm. For constructing an infinite propagation space, an impedance matching layer is set on the outer boundary of the ring-shaped array, so the propagation wave nearly has no reflection from the outer boundary.

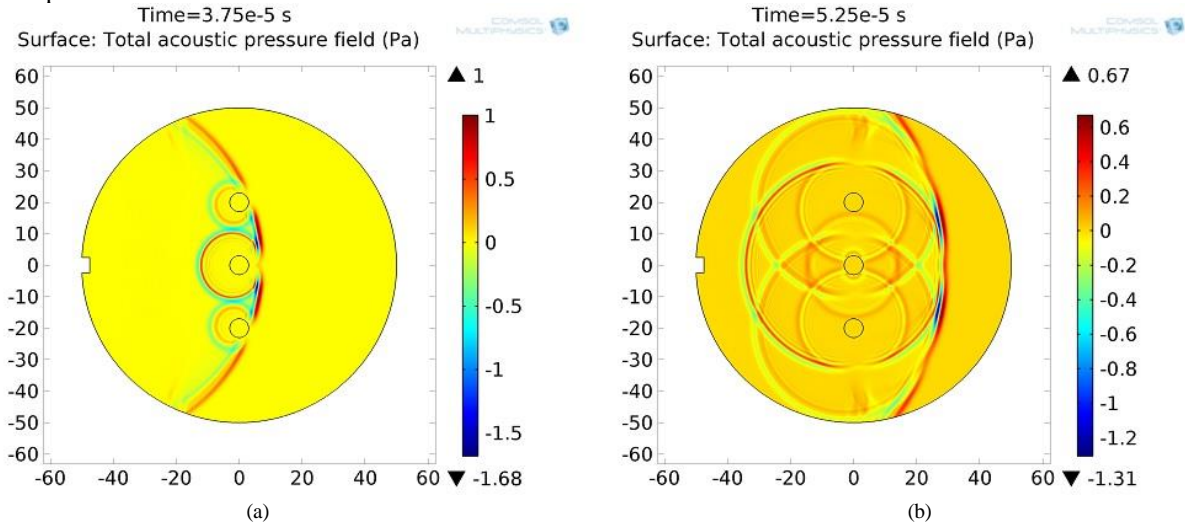


FIGURE 6 Transient distribution of the sound pressure interfered by 3 air bubbles inside the ring-shaped array (a). shows the refraction wave and the original reflection wave (b) shows the multiple reflection waves

3.2 IMAGE RECONSTRUCTION

Based on the concept of the previous sections, ultrasonic tomographic images are obtained. The reflected signals have a certain time width in general, so the full wave information including amplitudes and the propagation times can all be used to reconstruct the images.

Figure 7 shows the tested air bubbles and the

reconstructed image by ellipse algorithm. The 3 tested circle air bubbles with the radius of 3mm are longitudinal arranged inside the array from our viewing angle and the distances between the adjacent bubbles are all 20mm. The pressure of each bubble is set to be equal to the atmospheric pressure ($1.01e^5 Pa$) since the hydraulic pressure here is negligible, so the density of the bubble is $1.195kg/m^3$ (saturation state) and the speed of sound in the air bubble is $344m/s$.

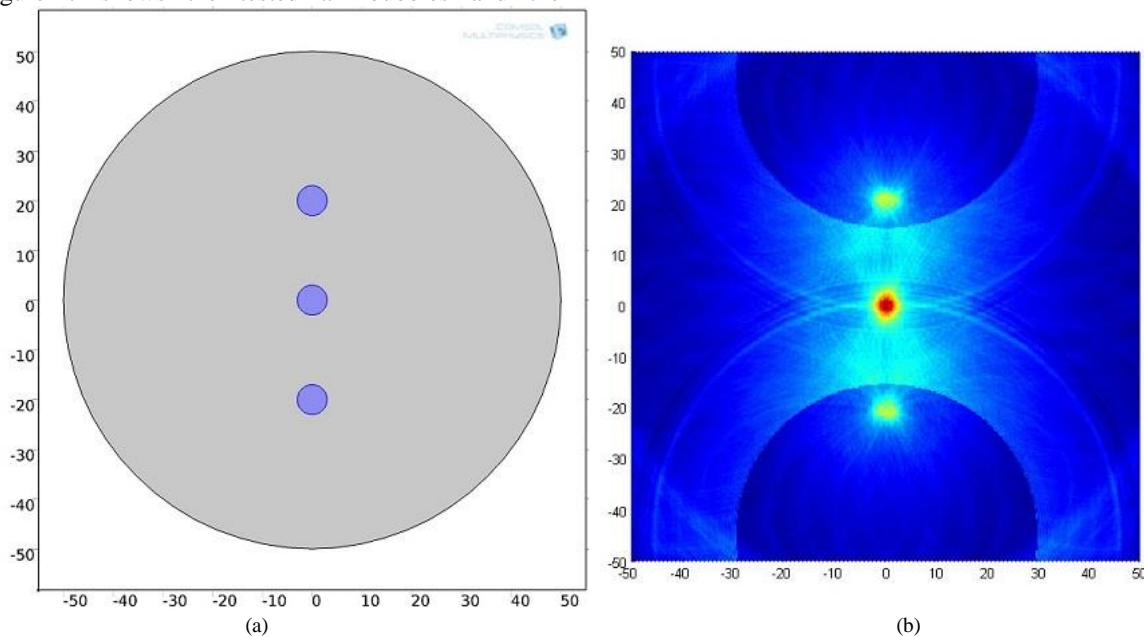


FIGURE 7 Three tested air bubbles and the corresponding reconstructed image obtained by ellipse algorithm (a). 3 tested circle air bubbles are longitudinal arranged within the immersion ultrasonic array, the radius of each bubble is 3mm and the distances between adjacent bubbles are 20mm. (b). The corresponding reconstructed image of 3 air bubbles

From the result displayed in Figure 7, reconstruction intensity of the imaged bubble located in the center of the array is higher than the other two bubbles, it shows that the

sensitivity of the ring-shaped array increases along with its radius and peak at its center.

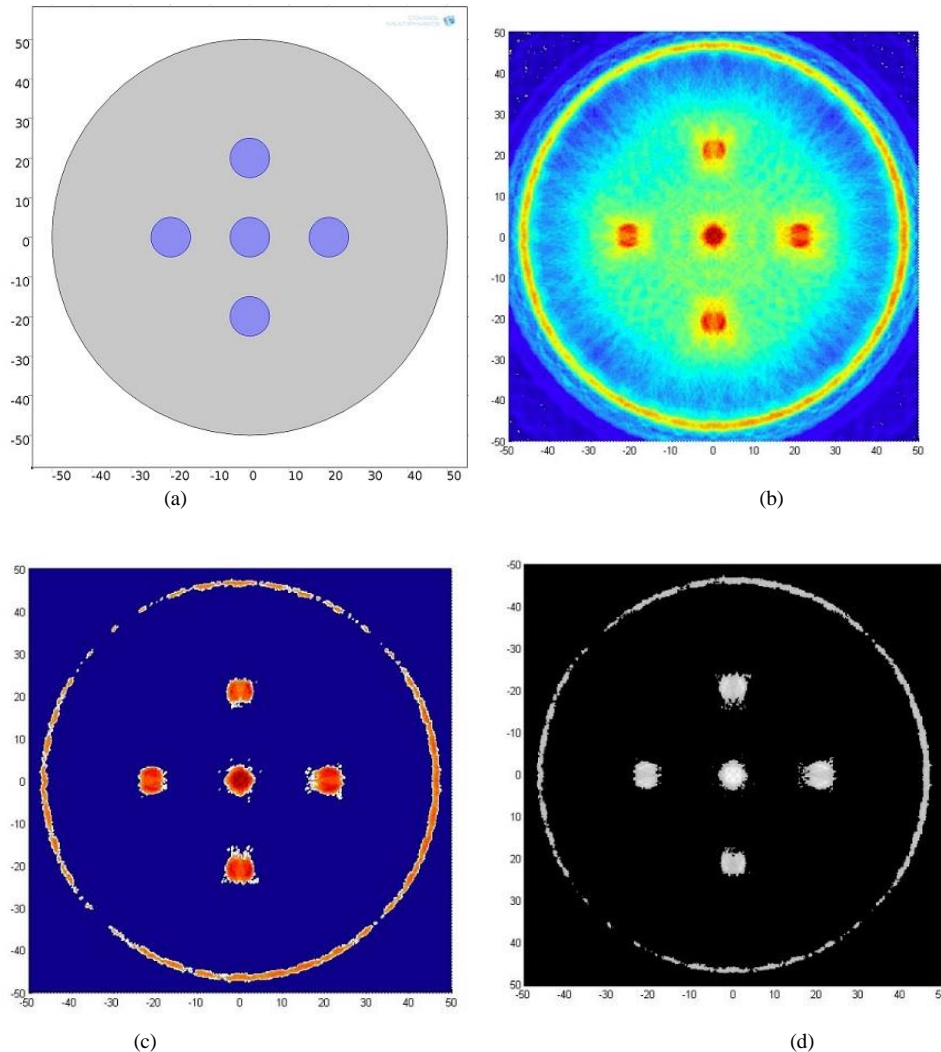


FIGURE 8 Five solid objects and the corresponding reconstructed images obtained by ellipse algorithm (a). 5 tested circle objects with the radius of 5mm are uniformly distributed around the center of the ring-shaped array. The horizontal distance and longitudinal distance of each solid object are all 20mm. (b). The corresponding reconstructed image of 5 solid objects. (c). The image after threshold filtering, in which the outlines of the objects can be seen clearly. (d). Grayscale image with better contrast

Figure 8 represents 5 solid objects with the radius of 5mm and their reconstructed images by ellipse algorithm. The horizontal distance and longitudinal distance of each solid object are all 20mm. the outer ring of the reconstructed image is resulted from the direct waves that are detected by all receiving transducers. Although the outer ring can be wiped off by adding an appropriate time-window to each receiving signal, the image quality inside the array will also be weakened because the direct waves are superimposed on part of the scattering signals.

The boundary outlines of 5 solid objects can be better observed by threshold filtering. Figure 8 (c) and (d) show the filtered image and the corresponding grayscale image. After filtering, the outlines of the solid objects are distinct and the contrast is enhanced.

4 Conclusions

The immersion ring-shaped array model for non-invasive ultrasonic tomography has been developed and investigated. After the simulation of ultrasonic propagation by COMSOL Multiphysics® software and the signal acquisition from each transducer, multi-objects images are reconstructed through ellipse algorithm. The image sizes reproduced by ellipse algorithm are smaller than the tested objects', but the images show the correct outlines which are closer to real. These phenomena are mainly resulted from the essence of ellipse algorithm, the superposition of a large number of ellipses. Reconstruction image of each single object might be interfered by others, because every trace of single ellipse can add pixels on their own paths. Much more effective approaches for improving the contrast and the resolution of the reconstructed images are increasing of frequency and transducer number.

References

- [1] Ohkawa, M., Kawata, N., Uchida, S. 1999 Cross-sectional distributions of gas and solid holdups in slurry bubble column investigated by ultrasonic computed tomography *Chemical Engineering Science* **54**(21), 4711-4728
- [2] Rahiman, M.H.F., Rahim, R.A., Tajjudin, M. 2006 Ultrasonic transmission-mode tomography imaging for liquid/gas two-phase flow *IEEE Sensors Journal* **6**(6), 1706-1715
- [3] Rahiman, M.H.F., Zakaria, Z., Rahim, R.A., Ng, W.N. 2009 Ultrasonic tomography imaging simulation of two-phase homogeneous flow *Sensor Review* **29**(3), 266-276
- [4] Alvarez, R.E., Macovski, A. 1976 Energy-selective reconstructions in x-ray computerised tomography *Physics in Medicine and Biology* **21**(5), 733
- [5] Momose, A., Takeda, T., Itai, Y., Hirano, K. 1996 Phase-contrast X-ray computed tomography for observing biological soft tissues *Nature medicine* **2**(4), 473-475
- [6] Zhao, Y., Brun, E., Coan, P., Huang, Z., Sztrókay, A., Diemoz, P.C., Liebhart, S., Mittone, A., Gasilov, S., Miao, J., Bravin, A. 2012 High-resolution, low-dose phase contrast X-ray tomography for 3D diagnosis of human breast cancers *Proceedings of the National Academy of Sciences* **109**(45), 18290-18294
- [7] Zeqiri, B., Baker, C., Alosa, G., Wells, P.N., Liang, H.D. 2013 Quantitative ultrasonic computed tomography using phase-insensitive pyroelectric detectors *Physics in medicine and biology* **58**(15), 5237
- [8] Hemzal, D., Peterlik, I., Jan, J., Rolecek, J. 2009 Experimental simulations of ultrasonic field time-development in 3D ultrasonic transmission tomography *The 9th International Conference on Information Technology and Applications in Biomedicine*, 1-4
- [9] Pintavirooj, C., Sangworasil, M. 2008 Ultrasonic Diffraction Tomography *International Journal of Applied Biomedical Engineering* **1**(1), 34-40
- [10] Hemzal, D., Peterlik, I., Rolecek, J., Jan, J., Ruiter, N., Jirik, R. 2008 3D simulation of diffraction in ultrasonic computed tomography *The 30th Annual International Conference of the IEEE Engineering in Medicine and Biology Society*, 454-457
- [11] Deleted by CMNT Editor
- [12] Deleted by CMNT Editor
- [13] Jeong, J.W., Shin, D.C., Do, S.H., Blanco, C., Klipfel, N.E., Holmes, D.R., Hovanessian-Larsen, L.J., Marmarelis, V.Z. 2008 Differentiation of cancerous lesions in excised human breast specimens using multiband attenuation profiles from ultrasonic transmission tomography *Journal of Ultrasound in Medicine* **27**(3), 435-451
- [14] Nebeker, J., Nelson, T.R. 2012 Imaging of sound speed using reflection ultrasound tomography *Journal of Ultrasound in Medicine* **31**(9), 1389-1404
- [15] Birk, M., Zapf, M., Balzer, M., Ruiter, N., Becker, J. 2014 A comprehensive comparison of GPU-and FPGA-based acceleration of reflection image reconstruction for 3D ultrasound computer tomography *Journal of Real-time Image Processing* **9**(1), 159-170
- [16] Deleted by CMNT Editor
- [17] Birk, M., Koehler, S., Balzer, M., Huebner, M., Ruiter, N.V., Becker, J. 2011 FPGA-Based Embedded Signal Processing for 3-D Ultrasound Computer Tomography *IEEE Transactions on Nuclear Science* **58**(4), 1647-1651
- [18] Ruiter, N., Schwarzenberg, G., Zapf, M., Gemmeke, H. 2008 Improvement of 3D ultrasound computer tomography images by signal pre-processing *Ultrasonics Symposium, IEEE*, 852-855
- [19] Ruiter, N.V., Göbel, G., Berger, L., Zapf, M., Gemmeke, H. 2011 Realization of an optimized 3D USCT *SPIE Medical Imaging* 796805
- [20] Ruiter, N.V., Zapf, M., Hopp, T., Dapp, R., Gemmeke, H. 2012 Phantom image results of an optimized full 3D USCT *SPIE Medical Imaging* 832005-1-832005-6
- [21] Yunus, F., Rahim, R., Aw, S., Ayob, N., Goh, C.L., Puspanathan, M. 2014 Simulation study of electrode size in air-bubble detection for dual-mode integrated electrical resistance and ultrasonic transmission tomography *Powder Technology* **256**, 224-232
- [22] Croxford, A.J., Wilcox, P.D., Drinkwater, B.W. 2008 Guided wave SHM with a distributed sensor network *Conference on Health Monitoring of Structural and Biological Systems* 69350E-1-69350E-9
- [23] Yang Liu, Xu Chunguang, Guo Xianghui. 2014. Ultrasonic Tomography of Immersion Circular Array by Hyperbola Algorithm *Journal of Engineering Science and Technology Review*, 2014, In Press

Authors	
	<p>< Yang Liu >, <1986.06>, < Datong City, Shanxi Province, P.R. China></p> <p>Current position, grades: PhD candidate of School of Mechanical Engineering, Beijing Institute of Technology, China.</p> <p>University studies: received his B.Sc. in School of Mechanical Engineering from China University of Mining and Technology in China.</p> <p>Scientific interest: His research interest fields include Ultrasonic imaging.</p> <p>Publications: more than 6 papers published in various journals.</p> <p>Experience: He has completed one scientific research projects.</p>
	<p>< Xu Chunguang >, <1964.05>, < Baoding City, Hebei Province, P.R. China></p> <p>Current position, grades: the professor of School of Mechanical Engineering, Beijing Institute of Technology, China.</p> <p>University studies: received his B.Sc., M.Sc. and Ph.D. in School of Mechanical Engineering from Beijing Institute of Technology in China.</p> <p>Scientific interest: His research interest fields include Non-destructive testing and evaluation.</p> <p>Publications: more than 100 papers published in various journals.</p> <p>Experience: He has teaching experience of 25 years, has completed ten scientific research projects.</p>
	<p>< Guo Xianghui >, <1982.11>, < Xinxiang City, Henan Province, P.R. China></p> <p>Current position, grades: PhD candidate of School of Mechanical Engineering, Beijing Institute of Technology, China.</p> <p>University studies: received his B.Sc. in School of Physics from Anyang Normal College, China. He received his M.Sc. in School of Physics from Beijing Institute of Technology, China.</p> <p>Scientific interest: His research interest fields include Ultrasonic testing and material reliability.</p> <p>Publications: more than 6 papers published in various journals.</p> <p>Experience: He has completed one scientific research projects.</p>